Available online at www.sciencedirect.com
SCIENCE DIRECT
International Journal of Mass Spectrometry 253 (2006) 274–280
International Journal of Mass Spectrometry
www.elsevier.com/locate/ijms

Distance dependence of through-bond electron transfer rates in electron-capture and electron-transfer dissociation

Monika Sobczyk, Jack Simons *

Chemistry Department and Henry Eyring Center for Theoretical Chemistry, University of Utah, Salt Lake City, Utah 84112, United States

Received 24 February 2006; received in revised form 29 April 2006; accepted 4 May 2006
Available online 12 June 2006

Abstract

Ab initio electronic structure calculations on model cations containing a disulfide linkage and a protonated amine site are carried out to examine how the rate of electron transfer from a Rydberg orbital on the amine site to the S–S σ* orbital depends upon the distance between these two orbitals. These simulations are relevant to both electron-capture and electron-transfer dissociation mass spectrometry where protonated peptide or protein samples are assumed to capture electrons in Rydberg orbitals of their protonated sites subsequent to which other bonds (especially S–S and N–C_α) are cleaved. By examining the dependence of three diabatic potential energy surfaces (one with an electron in the ground-state Rydberg orbital of the protonated amine, one with the electron in an excited Rydberg orbital on this same site, and the third with the electron attached to the S–S σ* orbital) on the S–S bond length, critical geometries are identified at which resonant through-bond electron transfer (from either of the Rydberg sites to the S–S σ* orbital) can occur. Landau–Zener theory is used to estimate these electron transfer rates for three model compounds that differ in the distance between the protonated amine and S–S bond sites. Once the electron reaches the S–S σ* orbital, cleavage of the S–S bond occurs, so it is important to characterize these electron transfer rates because they may be rate-limiting in at least some peptide or protein fragmentations. It is found that the Hamiltonian coupling matrix elements connecting each of the two Rydberg-attached states to the σ*-attached state decay exponentially with the distance between the Rydberg and σ* orbitals, so it is now possible to estimate the electron transfer rates for other similar systems.

Keywords: Through-bond; Electron transfer; Electron capture dissociation; Disulfide bond cleavage

1. Introduction

In recent publications [1], we performed theoretical simulations of the process in which an anion (A^-) having a low electron binding energy collides with a cation (M^+) containing a protonated amine site to effect electron transfer from A^- to M^+. Such processes are believed to occur in the promising new mass spectrometric approach to peptide and protein fragmentation termed electron-transfer dissociation (ETD) [2]. An example of the type of model system we studied in Refs. [1(a),(c)] is shown in Scheme 1 where cleavage of a disulfide linkage is the ultimate result of the electron transfer process.

If free electrons rather than an anion are used to neutralize a positive site in a peptide or protein, the mass spectrometric technique is termed electron-capture dissociation (ECD) [3]. Both ECD and ETD have proven to be very powerful tools for determining primary sequences in proteins and peptides. One of their especially desirable attributes is their ability to effect very specific bond cleavages throughout much of the backbone; the S–S and amide N–C_α bonds dominate the cleavages.

In our earlier studies in Ref. [1], the main focus was placed on estimating the cross-sections for transfer of the electron from the anion to either of three orbitals on the cation:

1. the lowest Rydberg orbital of the $-NH_3^+$ site,
2. the S–S σ* orbital, and
3. excited Rydberg orbitals of the $-NH_3^+$ site.

The key concept underlying how we estimated these cross-sections can be illustrated using the four potential energy curves shown qualitatively in Fig. 1.

* Corresponding author. Tel.: +1 801 581 8023.
E-mail address: simons@chem.utah.edu (J. Simons).
URL: http://simons.hec.utah.edu.

1387-3806/$ – see front matter © 2006 Elsevier B.V. All rights reserved.
doi:10.1016/j.ijms.2006.05.003

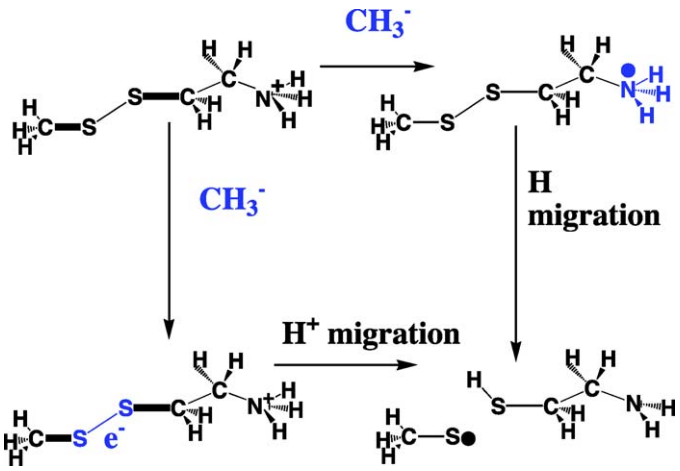

Scheme 1.

The potential curve that descends rapidly as the anion-to-nitrogen distance decreases represents the variation of the $H_3C–S–S–CH_2CH_2–NH_3^+ \cdots {}^-CH_3$ ion-pair state's energy. The three curves shown at lower energy having very weak dependence on the anion-to-nitrogen distance represent the variation of the $H_3C–S^-–S–CH_2CH_2–NH_3\cdots CH_3$ state (with the electron transferred to the S–S σ* orbital), the $H_3C–S–S–CH_2CH_2–NH_3\cdots CH_3$ state (with the electron in an excited Rydberg orbital on the $–NH_3$ site), and the $H_3C–S–S–CH_2CH_2–NH_3\cdots CH_3$ state (with the electron in the ground-state Rydberg orbital on the $–NH_3$), respectively. At the critical distances where the ion-pair potential curve crosses each of the other three curves, resonant electron transfer is assumed to occur. The cross-sections of these resonant electron transfer reactions were evaluated using Landau–Zener theory in Ref. [1]. One of the primary conclusions of this earlier work was that the cross-section for direct (i.e., in the collision) electron transfer to the S–S σ* orbital (or to the C=O π* orbital of an amide site in a peptide bond) is one to two orders of magnitude smaller than for transfer to either the ground- or excited-Rydberg orbitals. We thus concluded that in ETD experiments, electron transfer is most likely to occur to the protonated sites, although transfer to disulfide or amide sites can occur with lower probability.

In our most recent study [1a], we also considered what happens after collisional electron transfer to a protonated site. In particular, we asked whether the attached electron could migrate from the $–NH_3$ site into the S–S σ* orbital and thus fragment the S–S bond in this way. We addressed this issue by examining the variation of three electron-attached states' energies as the S–S bond length varies:

1. the $H_3C–S^-–S–CH_2CH_2–NH_3\cdots CH_3$ state (with the electron transferred to the S–S σ* orbital),
2. the $H_3C–S–S–CH_2CH_2–NH_3\cdots CH_3$ state (with the electron in an excited Rydberg orbital on the $–NH_3$ site), and
3. the $H_3C–S–S–CH_2CH_2–NH_3\cdots CH_3$ state (with the electron in the ground-state Rydberg orbital on the $–NH_3$).

For the model compound $H_3C–S–S–CH_2CH_2–NH_3^+$ used in Ref. [1a], these states' potential curves are shown in Fig. 2 (calculated at the second-order Møller–Plesset (MP2) level).

At the top of Fig. 2 we also show the S–S σ* orbital (left), the first excited Rydberg orbital (middle) and the ground Rydberg orbital (right) for an S–S distance of 2.6 Å. The contour lines have been chosen so that 60% of the total electron density within each orbital is contained within the volume outlined by

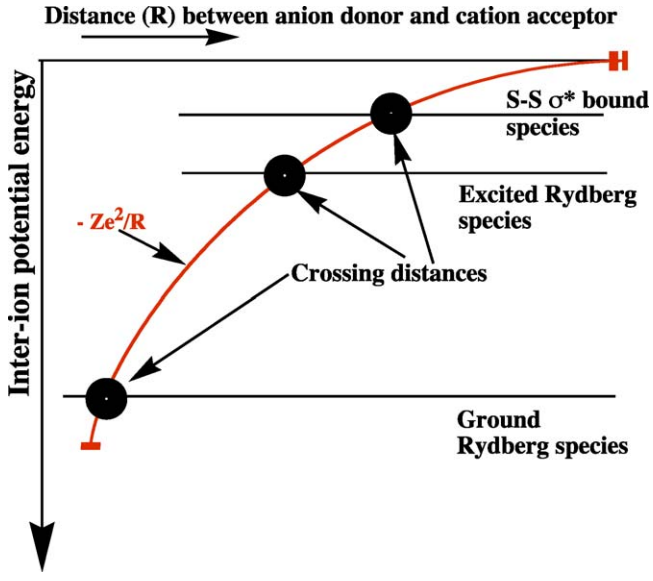

Fig. 1. Qualitative depiction of the variation of the four cation-anion state energies as functions of the anion-to-nitrogen distance *R*.

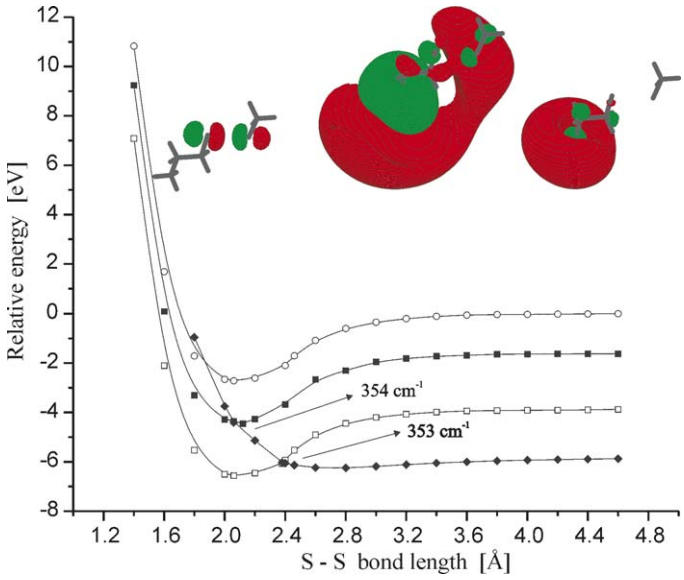

Fig. 2. MP2-level energies of the parent cation (open circles) and of the species in which an electron is attached to the ground-Rydberg orbital (open squares), the excited-Rydberg orbital (filled squares), or the S–S σ* orbital (filled diamonds) as functions of the S–S bond length. The MP2-level $H_{1,2}$ coupling matrix elements are also shown near the respective surface crossing points, and the S–S σ*, excited, and ground Rydberg orbitals (at $R = 2.6$ Å) are shown on the top from left to right.

the outermost contour. It is important to notice that the two Rydberg orbitals have quite large spatial extent that causes them to significantly overlap the region of the S–S bond. As a result, the ground-state Rydberg orbital contains a (small) component of S–S σ* character, and the excited Rydberg orbital contains significantly more S–S σ* character. These differences are reflected in the differences in the through-bond electron transfer couplings that we compute and discuss later in this paper.

In the regions near 2.1 and 2.4 Å where the dissociative S–S σ*-attached curve intersects the excited- and ground-Rydberg curves, respectively, we also evaluated the Hamiltonian coupling matrix elements $H_{1,2}$ between the pairs of intersecting curves. This was done by computing the adiabatic Born–Oppenheimer energies at several *R*-values (at a much finer spacing than shown in Fig. 2) and determining the *R*-value at which the pairs of adiabatic curves had the smallest energy difference. $H_{1,2}$ was then taken to be one-half of this minimum spacing, and these values are shown in Fig. 2. Of course, we also verified that the adiabatic curves, in the region of minimum spacing, were indeed strongly mixed combinations of S–S σ* and Rydberg (excited or ground) orbital character.

Once we had the $H_{1,2}$ matrix elements we were able to evaluate the rates at which a nascent Rydberg-attached (excited or ground) electron could migrate, by surface hopping, to the S–S σ* orbital and thus effect S–S bond cleavage. The details of how we again used Landau–Zener theory to carry out these rate estimates are given in Ref. [1a]. The final result was a prediction that (at room temperature), the rate of transitions from the excited Rydberg state to the σ* state will be ca. $10^{12}\ s^{-1}$ (i.e., requiring only a few vibrations of the S–S bond) while the rate of transitions from the ground Rydberg state will be many orders of magnitude smaller. The factor that greatly reduces the rate for the ground Rydberg state is that to access the crossing with the S–S σ* curve near 2.4 Å requires substantial vibrational excitation of the S–S bond whereas the crossing for the excited Rydberg state near 2.1 Å occurs much closer to the S–S bond's zero-point vibrational energy.

In the present paper, we extend the study of Ref. [1a] by examining the dependence of the $H_{1,2}$ coupling matrix elements on distance within a series of three model compounds $H_3C–S–S–(CH_2)_n–NH_3^+$ with $n = 1,2$, and 3. By examining the potential curves of the family of electron-attached states (analogous to those shown in Fig. 2) as functions of the S–S bond length, we could then evaluate the rates at which intra-molecular electron transfer from a Rydberg (ground or excited) orbital to the S–S σ* orbital can take place. In this way, we are able to estimate the rates of S–S bond cleavage for the two Rydberg states and for all three ($n = 1$, 2, 3) model compounds. By constraining the geometry of the model systems, we can keep fixed the distance from the mid-point of the S–S bond to the centroid of the Rydberg orbital and thus gain insight into the distance-dependence of the $H_{1,2}$ matrix elements and thus of the electron transfer rates.

In Section 2, we describe the methods we use to carry out the simulations, and in Section 3, we present and discuss our findings. Section 4 contains a summary of the results presented here.

2. Methods

The internal structure (bond lengths and angles) of the parent $H_3C–S–S–(CH_2)_n–NH_3^+$ cation was first optimized at the Hartree-Fock (HF) self-consistent field (SCF) level and subsequently held fixed throughout our calculations characterizing the collisions with the $–CH_3$ anion. We froze the internal geometry of these cations because we are attempting to model the environment within a peptide or protein in which an S–S σ* orbital is Coulomb stabilized by a positively charged site whose location remains quite fixed. In addition, we wanted to extract information about the distance-dependence of the electron transfer rates, so it was important to have the distance from the S–S bond to the $–NH_3^+$ site held fixed.

We should note that in most peptides and proteins, protonated amine groups are likely to be involved in hydrogen bonds (e.g., to nearby amide carbonyl groups), unlike the $–NH_3^+$ group in our model compound. This, no doubt, will somewhat alter the energies and shapes of the protonated amine site's Rydberg orbitals. Therefore, it is important to not view the quantitative data (e.g., through-bond coupling strengths and electron transfer rates) obtained here as representative of any specific peptide. Rather, our study is designed to suggest that in real protonated peptides and proteins, all of which possess a rich family of Rydberg states, it is likely that at least one such Rydberg state will have its potential surface crossed by the S–S σ* surface near the former's minimum and thus be able to effect electron transfer to the S–S σ* orbital. In addition, our study shows, as we illustrate later, that the magnitudes of the through-bond couplings between ground or excited Rydberg states are large enough to suggest that transfer to S–S bonds as far as 10–12 Å from the protonated site can occur.

To properly describe the ground and excited Rydberg states of the $R–NH_3$ species we added to the aug-cc-pVDZ basis sets [4] an additional set (1s1p) of extra diffuse functions [5] centered on the nitrogen atom. This kind of basis was shown earlier [5] to be capable of reproducing the energies of such low Rydberg states of nitrogen-centered radicals. Because we have only four such extra diffuse functions in our basis, the number of Rydberg levels that we can describe is limited. As noted earlier, any real protonated peptide has an infinite progression of Rydberg states. So, the present study in which we explore only a few such states can only offer suggestive evidence about the strengths of through-bond couplings and electron transfer rates that are likely to occur in actual peptide or protein samples.

To generate the four energy surfaces ($H_3C–S–S–(CH_2)_n–NH_3^+$, $H_3C–S–S–(CH_2)_n–NH_3$ ground Rydberg, $H_3C–S–S–(CH_2)_n–NH_3$ excited Rydberg, and $H_3C–S–S–(CH_2)_n–NH_3$ S–S σ*) needed to evaluate the cross-sections for electron transfer, we performed calculations at the unrestricted second-order Møller-Plesset (UMP2) level and examined the energies of the ground-Rydberg, excited-Rydberg, and S–S σ*-attached states as functions of the S–S bond length (with the other internal coordinates of $H_3C–S–S–(CH_2)_n–NH_3$ held fixed for the reasons noted earlier). The use of an unrestricted method was necessary both to achieve a qualitatively correct description of the

homolytic cleavage of the S–S bond and because the various electron-attached $H_3C–S–S–(CH_2)_n–NH_3$ species are open-shell systems.

Because the methods we used are based on an unrestricted Hartree-Fock starting point, it is important to make sure that little, if any, artificial spin contamination enters into the final wave functions. We computed the expectation value $\langle S^2 \rangle$ for species studied in this work and found values not exceeding (after annihilation) the expected value of 0.75 by more than 0.05 in all open-shell doublet neutral cases.

The calculations we performed are especially problematic because we need to compute the energies of not just the lowest-energy electron-attached state at each S–S bond length, but the energies of three such states. In such cases, great care must be taken to avoid variational collapse. For the ground-Rydberg state, this was not an issue, but it was for the excited-Rydberg state. For this case, we found it adequate to use the "alter" option in the Gaussian program to begin the iterative SCF process with the desired orbital occupancy. Convergence to the desired (excited Rydberg) state was then verified by visually inspecting the singly occupied orbital after convergence.

For the state in which the electron is attached to the S–S σ* orbital, the "alter" option did not work (i.e., variational collapse took place during the SCF iterations), so we had to use another approach. In the method we used to overcome the problem for this state, we introduced a device that we have exploited in many past applications [6]. Specifically, we artificially increased the nuclear charges by a small amount δq of the atoms (the sulfur atoms for the S–S σ* state or the nitrogen atom for the ground and excited Rydberg states) involved in accepting the transferred electron and carried out the UMP2 calculations with these artificial nuclear charges. By plotting the energies of the states of $H_3C–S–S–(CH_2)_n–NH_3$ for several values of the charge increment δq and extrapolating to $\delta q = 0$, we were able to evaluate the true energy of the $H_3C–S–S–(CH_2)_n–NH_3$ states. To our knowledge, this method was pioneered by the Peyerimhoff group [7] and has proven useful in a variety of situations. Finally, the Gaussian 03 suite of programs [8] was used to perform all of the calculations, and Molden visualization program [9] was employed to examine the molecular orbitals.

3. Results and discussion

In Figs. 2 and 3 we display the variations of the energies of the parent $H_3C–S–S–(CH_2)_n–NH_3^+$ cations and of the three electron-attached states (i.e., ground and excited Rydberg and S–S σ*) as functions of the S–S bond length. In these figures we also show the two Rydberg and the S–S σ* orbitals (at an S–S distance of 2.6 Å) as well as the values of the $H_{1,2}$ coupling matrix elements we extracted from the adiabatic Born-Oppenheimer curves. Notice that the Rydberg orbitals for the longer ($n = 3$) structure shown in the top of Fig. 3 do not possess as much S–S σ* character as the corresponding Rydberg orbitals for $n = 2$ shown in Fig. 2. On the other hand, the Rydberg orbitals of the shortest species ($n = 1$) are even more strongly coupled to the S–S σ* orbital as seen in the bottom of Fig. 3.

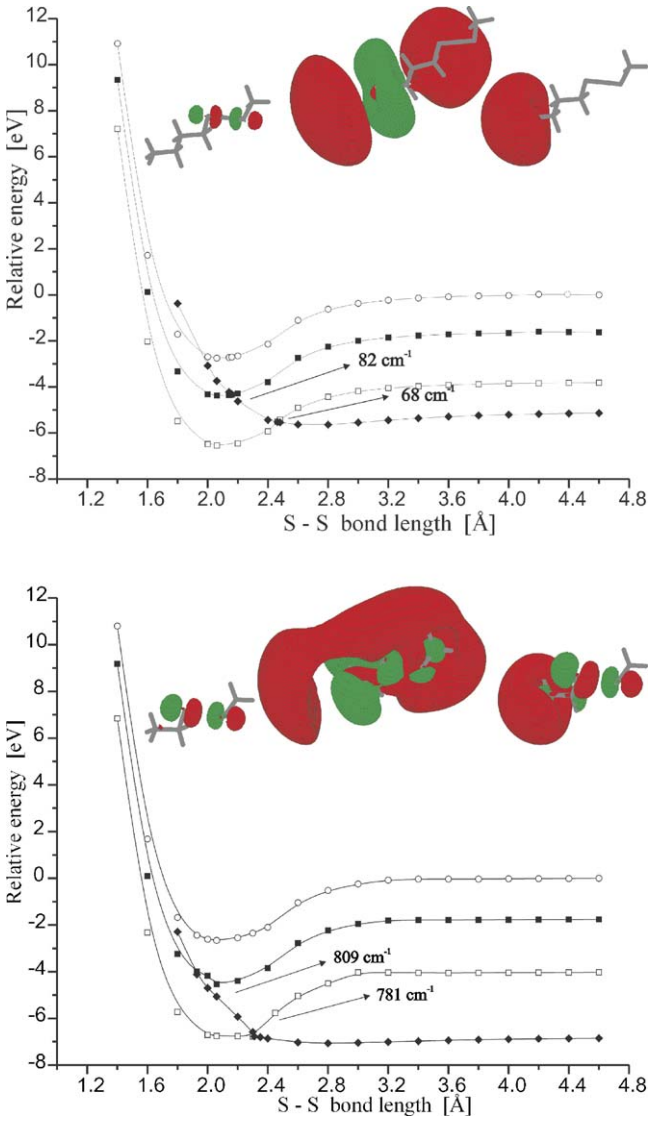

Fig. 3. MP2-level energies of the parent $H_3C–S–S–(CH_2)_n–NH_3$ cations (open circles) and of the species in which an electron is attached to the ground-Rydberg orbital (open squares), the excited-Rydberg orbital (filled squares), or the S–S σ* orbital (filled diamonds) as functions of the S–S bond length. The top figure is for $n = 3$ and the bottom is for $n = 1$; Fig. 2 gives the corresponding data for $n = 2$. The MP2-level $H_{1,2}$ coupling matrix elements are also shown as are the S–S σ*, excited and ground-state Rydberg orbitals from left to right.

The first observation we make about the curves shown in Figs. 2 and 3 is that the relative energy-spacings and shapes of the parent cation and the two Rydberg-attached curves are essentially independent of how many $–CH_2$-groups are present. In contrast, the relative energies (but not the shapes) of the S–S σ*-attached curves depend on how many methylene units are present. These data are, of course, not surprising because the energy of the S–S σ* orbital depends on the distance to the $–NH_3^+$ positive site that provides the Coulomb stabilization to render exothermic the electron attachment to this σ* orbital as we showed in earlier works [1].

The primary implications of the variation of the S–S σ* curve with the number of methylene units are that:

1. The locations of the crossings of the σ* and Rydberg curves evolve to larger *R*-values as the number of methylene units increases, and
2. The magnitudes of the $H_{1,2}$ matrix elements (for both ground and excited Rydberg states coupling to the σ* state) decrease as the number of methylene units increases. Consistent with the latter observation is the fact that the adiabatic Born-Oppenheimer states contain larger admixtures of the Rydberg and S–S σ* orbitals for the system containing only one methylene unit than for the other two systems. This can be seen by examining the adiabatic molecular orbitals shown in Figs. 2 and 3 for the three model molecules. Another way to view the trend in where the crossings occur is that, as the number of methylene units increases, that Rydberg state which undergoes a crossing with the S–S σ* state near the Rydberg's minimum will be a higher and higher energy Rydberg state.

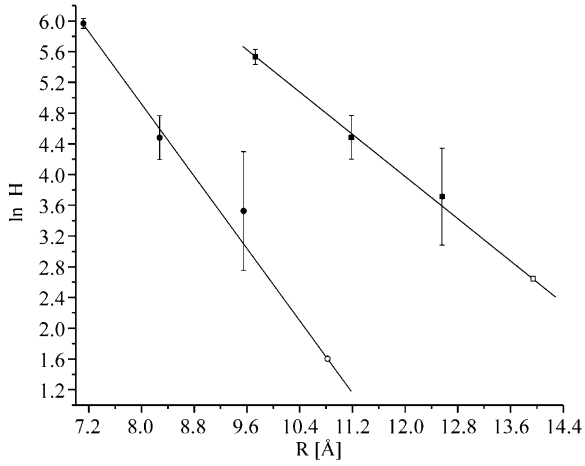

Fig. 4. Variation of the $H_{1,2}$ coupling matrix elements as functions of the distance *R* between the mid-point of the S–S bond and the centroid of the Rydberg orbital (ground or excited) for the ground (left) and excited (right) Rydberg state coupling to the S–S σ* state. The error bars indicate 50 cm^{-1} uncertainty in the values of the $H_{1,2}$ elements. The open square symbols show the value of $\ln H_{1,2}$ obtained by extrapolation to a compound containing 4 methylene units.

Having extracted the $H_{1,2}$ matrix elements from our UMP2-level adiabatic Born–Oppenheimer curves, we decided to see whether they varied in the expected [10] exponential manner with the distance between the two sites between which the electron migrates. Therefore, in Fig. 4 we show plots of the $H_{1,2}$ data for the ground-Rydberg to S–S σ* and excited-Rydberg to S–S σ* electron transfer events. Because, as one sees in Figs. 2 and 3, the Rydberg orbitals are quite delocalized, it is difficult to define a unique distance parameter (*R*) to employ in plotting the $\ln H_{1,2}$ data. We have chosen to use the distance between the mid-point of the S–S bond and the centroid [11] of the (ground or excited) Rydberg orbital as the variable *R* plotted on the horizontal axis of Fig. 4. We estimated the uncertainties in the $H_{1,2}$ matrix elements resulting from our limited ability to identify the precise S–S bond length at which the two adiabatic curves have their minimum spacing to be 50 cm^{-1}, and error bars based on this estimate are shown in Fig. 4.

It appears that the through-bond electron transfer couplings $H_{1,2}$ do indeed fit the expected exponential form. Linear fits to our $H_{1,2}$ data produce equations of the form $\ln H_{1,2} = 14.33 - 1.18R$ for the ground Rydberg state and $\ln H_{1,2} = 12.18 - 0.68R$ for the excited Rydberg state, with *R* in Å. Extrapolating these fits to an $n = 4$ model compound having one more methylene unit gives predicted $H_{1,2}$ values of 5 cm^{-1} for the ground Rydberg state and 14 cm^{-1} for the excited Rydberg state. It is impossible to accept these two estimates as being quantitatively accurate, given our suggested 50 cm^{-1} errors in evaluating the calculated $H_{1,2}$ data. However, the observed nearly exponential decay of the $H_{1,2}$ data suggest that the $n = 4$ $H_{1,2}$ values should be ca. an order of magnitude smaller than those for $n = 3$.

Having these matrix elements in hand, we also computed the rates at which electron transfer is expected to occur between the ground or excited Rydberg state and the S–S σ*-attached state for $n = 1$, 2, and 3. In Table 1, we present these rates, which have been computed as in Ref. [1a] and as briefly summarized below.

The rates shown in Table 1 were computed by multiplying the frequency ν of vibration of the S–S bond (we computed this to be 562 cm^{-1} or ca. 2×10^{13} s^{-1}) by the thermal probability *p* that the S–S bond's vibration is sufficiently excited to access the (ground or excited) Rydberg-σ* crossing point and by the probability *P* that a surface hop will occur from the Rydberg state to the S–S σ*-attached state.

The probability that the S–S bond is in vibrational level *v* is $\exp(-h\nu(v + 1/2)/kT)/q_{vib}$, where q_{vib} is the vibrational partition function for this mode: $q_{vib} = \exp(-h\nu/2kT)/(1 - \exp(-h\nu/kT))$. The probability *p* that the S–S vibration is in

Table 1
Rates of intra-molecular through-bond electron transfer for three model compounds and two Rydberg states (s^{-1}) and hopping and thermal probabilities

Species	Coupled states	Rate (s^{-1})	Hopping[a] probability *P*	Thermal[b] probability *p*
$H_3C{-}SS{-}CH_2{-}NH_3$	Ground Rydberg and SS σ*	9.8×10^{10}	0.45	1.3×10^{-2}
$H_3C{-}SS{-}CH_2{-}NH_3$	Excited Rydberg and SS σ*	1.1×10^{6}	0.61	1.0×10^{-7}
$H_3C{-}SS{-}CH_2{-}CH_2{-}NH_3$	Ground Rydberg and SS σ*	1.1×10^{4}	0.13	5.2×10^{-9}
$H_3C{-}SS{-}CH_2{-}CH_2{-}NH_3$	Excited Rydberg and SS σ*	7.9×10^{11}	0.51	9.2×10^{-2}
$H_3C{-}SS{-}CH_2{-}CH_2{-}CH_2{-}NH_3$	Ground Rydberg and SS σ*	2.2×10^{-7}	0.004	3.2×10^{-18}
$H_3C{-}SS{-}CH_2{-}CH_2{-}CH_2{-}NH_3$	Excited Rydberg and SS σ*	3.1×10^{11}	0.054	3.4×10^{-1}

[a] Defined in Eq. (2).
[b] Defined in Eq. (1) and evaluated for $T = 300$ K.

or above the lowest level $v*$ whose motion accesses the crossing point can be computed as

$$p = \sum_{v^*}^{\infty} \exp \frac{(-h\nu(v + 1/2)/kT)}{q_{\text{vib}}} = \exp\left(\frac{-h\nu v*}{kT}\right) \quad (1)$$

Alternatively, $h\nu v*$ gives the minimum energy E^* (above zero-point) needed to access the crossing point, and p can be expressed as $p = \exp(-E^*/kT)$. To gain a feeling for how this factor affects the electron transfer rate, we can use our computed harmonic S–S vibrational frequency (562 cm^{-1}) and note that at 300 K, kT corresponds to 0.59 kcal mol^{-1} or 208 cm^{-1} to evaluate the factor $\exp(-h\nu v*/kT)$ as 0.067 for $v* = 1$ and 9×10^{-8} for $v* = 6$. These thermal probability factors (for $T = 300$ K) appropriate to the curve crossings shown in Figs. 2 and 3 are given in Table 1.

The surface hopping probabilities P were computed using Landau–Zener (LZ) theory as

$$P = 1 - \exp\left[\frac{-2\pi {H_{1,2}}^2}{(\hbar v \delta F)}\right], \quad (2)$$

where $H_{1,2}$ is the coupling matrix element, δF is the difference in slopes for the (ground or excited) Rydberg and σ* curves at their crossing and v is the speed at which the S–S bond moves through the crossing point. The speeds v have been estimated as follows. We know the frequency ν of the S–S vibration and, for any vibrational level v, we can evaluate the left and right turning points for this bond's oscillatory motion. Using twice the distance between the left and right turning points times the frequency ν, we can estimate the (average) speed at which the S–S bond is moving [12].

For the model compounds with 1 or 2 methylene units, the hopping probabilities evaluated using Eq. (2) are substantial fractions of unity (e.g., 0.13–0.61), which means that not too many S–S vibrational periods are needed to effect electron transfer (as long as the S–S bond is sufficiently excited to access the crossing point which is what the thermal probability p measures). Moreover, for both of these model compounds, either the ground or excited Rydberg state crosses the σ* state at a geometry with a favorable thermal probability factor (P-see Table 1). As a result, the Rydberg-to-σ* electron transfer rates are ca. 10^{11}–10^{12} s^{-1} for the $n = 1$ and 2 compounds.

For the compound with three methylene units, the hopping probabilities are 0.004 and 0.054 (because the $H_{1,2}$ elements are 4–5 times smaller than for the $n = 2$ case). Moreover, only the excited Rydberg state accesses the crossing with the σ* state at a geometry with a favorable thermal probability factor. Nevertheless, the electron transfer rate for this compound (ca. 10^{11} s^{-1} for the excited Rydberg state) are similar to those for $n = 1$ and 2 (see Table 1).

What do these findings suggest will occur more generally? We expect that for any number of methylene units (i.e, any distance between the S–S bond and the $-NH_3^+$ site), there will be one or more Rydberg state for which the crossing with the σ* state occurs in the thermally vibrationally accessible region. For this state, the rate of electron transfer will be governed primarily by the ${H_{1,2}}^2$ factor entering into the surface hopping probability factor. Moreover, once distances greater than those appearing in the $n = 3$ case studied here are appropriate, these surface hopping probabilities can be approximated by the linearized version of Eq. (2):

$$P = \frac{2\pi {H_{1,2}}^2}{(\hbar v \delta F)}. \quad (3)$$

This suggests then that the rates will scale with ${H_{1,2}}^2$, as expected and can be estimated by multiplying the probability given in Eq. (3) by the rate of vibration of the S–S bond (i.e., assuming the thermal probability factor p is near unity).

4. Summary

The primary conclusions of this work are that:

1. Subsequent to electron attachment (via either electron transfer from an anion in a collision or by attachment of a free electron) to a positively charged amine $-NH_3^+$ site, through-bond electron transfer to an S–S σ* orbital can occur. Although we have only examined transfer through methylene units to date, we intend to examine other through-bond transfers (e.g., involving peptide bond linkages) in future efforts.
2. The rate of the through-bond transfer is ca. 10^{11} s^{-1} for compounds with as many as three methylene units, and thus only a few to a hundred S–S bond vibrations are needed to effect transfer.
3. If the $-NH_3^+$ site is close enough to render exothermic the electron attachment to the S–S σ* orbital (ca. 14 Å or closer), there will exist a $-NH_3^+$ site Rydberg state (ground or excited) whose energy profile will cross that of the S–S σ* anion near the equilibrium S–S bond length of the parent cation.
4. Electron transfer from this Rydberg state to the S–S σ* orbital will be governed by the surface-hopping probability (Eqs. (2) and (3)) which, in turn, depends quadratically on the Hamiltonian coupling elements $H_{1,2}$ determined for three model compounds in this work.
5. The magnitude of the $H_{1,2}$ element is found to decay exponentially with the distance R between the S–S bond midpoint and the centroid of the Rydberg orbital from which the electron is transferred. The functional form of this dependence was determined to be $\ln H_{1,2} = 14.33 - 1.18R$ for the ground Rydberg state and $\ln H_{1,2} = 12.18 - 0.68R$ for the excited Rydberg state, with R in Å.

In summary, the results obtained on the model systems studied here suggest a mechanism for S–S bond cleavage in which

a. An electron is captured into a high Rydberg state of a protonated amine site;
b. relaxation (radiationless or radiative) to lower Rydberg states follows until;
c. a critical Rydberg state is reached (that whose potential surface is crossed by the S–S σ* state near the Rydberg state's minimum);

d. then, through-bond electron transfer from this critical Rydberg state to the S–S σ* state can occur at rates;
e. that are determined by the $H_{1,2}{}^2$ elements connecting the Rydberg and σ* states.

They also suggest that the $H_{1,2}$ values fall off exponentially with the distance between the σ* and Rydberg orbitals but that the fall off is slow enough to permit migration through at least 10–12 Å (for methylene units) at rates of 10^{11} s^{-1}.

Acknowledgements

Support of the National Science Foundation through grant CHE 0240387 is appreciated. Significant computer time provided by the Center for High Performance Computing at the University of Utah and by the Academic Computer Center in Gdansk (TASK) is also gratefully acknowledged. We also thank Dr. Thomas Sommerfeld for allowing us to use his program for determining the fractional electron density within MOLDEN plots.

References

[1] (a) M. Sobczyk, J. Simons, J. Phys. Chem. B 110 (2006) 7519;
(b) I. Anusiewicz, J. Berdys-Kochanska, P. Skurski, J. Simons, J. Phys. Chem. A 110 (2006) 1261;
(c) I. Anusiewicz, J. Berdys-Kochanska, J. Simons, J. Phys. Chem. A 109 (2005) 5801.

[2] (a) J.E.P. Syka, J.J. Coon, M.J. Schroeder, J. Shabanowitz, D.F. Hunt, Proc. Natl. Acad. Sci. 101 (2004) 9528;
(b) J.J. Coon, J.E.P. Syka, J.C. Schwartz, J. Shabanowitz, D.F. Hunt, Int. J. Mass Spectrom. 236 (2004) 33;
(c) S.J. Pitteri, P.A. Chrisman, S.A. McLuckey, Anal. Chem. 77 (2005) 5662;
(d) H.P. Gunawardena, M. He, P.A. Chrisman, S.J. Pitteri, J.M. Hogan, B.D.M. Hodges, S.A. McLuckey, J. Am. Chem. Soc. 127 (2005) 12627.

[3] (a) R.A. Zubarev, N.L. Kelleher, F.W. McLafferty, J. Am. Chem. Soc. 120 (1998) 3265;
(b) R.A. Zubarev, N.A. Kruger, E.K. Fridriksson, M.A. Lewis, D.M. Horn, B.K. Carpenter, F.W. McLafferty, J. Am. Chem. Soc. 121 (1999) 2857;
(c) R.A. Zubarev, D.M. Horn, E.K. Fridriksson, N.L. Kelleher, N.A. Kruger, M.A. Lewis, B.K. Carpenter, F.W. McLafferty, Anal. Chem. 72 (2000) 563;
(d) R.A. Zubarev, K.F. Haselmann, B. Budnik, F. Kjeldsen, F. Jensen, Eur. J. Mass Spectrom. 8 (2002) 337;
(e) Much of the pioneering work aimed at understanding the mechanism(s) by which ECD operates has been reported in refs. 3a–d and by the Turecek and Uggerud groups in, for example, the following: E.A. Syrstad, F. Turecek, J. Phys. Chem. A 105 (2001) 11144;
(f) F. Turecek, E.A. Syrstad, J. Am. Chem. Soc. 125 (2003) 3353;
(g) F. Turecek, M. Polasek, A. Frank, M. Sadilek, J. Am. Chem. Soc. 122 (2000) 2361;
(h) E.A. Syrstad, D.D. Stephens, F. Turecek, J. Phys. Chem. A 107 (2003) 115;
(i) F. Turecek, J. Am. Chem. Soc. 125 (2003) 5954;
(j) E.A. Syrstad, F. Truecek, J. Am. Soc. Mass. Spectrom. 16 (2005) 208;
(k) E. Uggerud, Int. J. Mass. Spectrom. 234 (2004) 45.

[4] R.A. Kendall, T.H. Dunning Jr., R.J. Harrison, J. Chem. Phys. 96 (1992) 6796.

[5] (a) M. Gutowski, J. Simons, J. Chem. Phys. 93 (1990) 3874;
(b) P. Skurski, M. Gutowski, J. Simons, Int. J. Quantum Chem. 80 (2000) 1024.

[6] See, for example, the description offered in I. Anusiewicz, J. Berdys, M. Sobczyk, A. Sawicka, P. Skurski, J. Simons, J. Phys. Chem. A 109 (2005) 250.

[7] See, for example, B. Nestmann, S.D. Peyerimhoff, J. Phys. B 18 (1985) 615;
B. Nestmann, S.D. Peyerimhoff, J. Phys. B 18 (1985) 4309.

[8] M.J. Frisch, G.W. Trucks, H.B. Schlegel, G.E. Scuseria, M.A. Robb, J.R. Cheeseman, J.A. Montgomery, Jr., T. Vreven, K.N. Kudin, J.C. Burant, J.M. Millam, S.S. Iyengar, J. Tomasi, V. Barone, B. Mennucci, M. Cossi, G. Scalmani, N. Rega, G.A. Petersson, H. Nakatsuji, M. Hada, M. Ehara, K. Toyota, R. Fukuda, J. Hasegawa, M. Ishida, T. Nakajima, Y. Honda, O. Kitao, H. Nakai, M. Klene, X. Li, J.E. Knox, H.P. Hratchian, J.B. Cross, C. Adamo, J. Jaramillo, R. Gomperts, R.E. Stratmann, O. Yazyev, A.J. Austin, R. Cammi, C. Pomelli, J.W. Ochterski, P.Y. Ayala, K. Morokuma, G.A. Voth, P. Salvador, J.J. Dannenberg, V.G. Zakrzewski, S. Dapprich, A.D. Daniels, M.C. Strain, O. Farkas, D.K. Malick, A.D. Rabuck, K. Raghavachari, J.B. Foresman, J.V. Ortiz, Q. Cui, A.G. Baboul, S. Clifford, J. Cioslowski, B.B. Stefanov, G. Liu, A. Liashenko, P. Piskorz, I. Komaromi, R.L. Martin, D.J. Fox, T. Keith, M.A. Al-Laham, C.Y. Peng, A. Nanayakkara, M. Challacombe, P.M.W. Gill, B. Johnson, W. Chen, M.W. Wong, C. Gonzalez, and J.A. Pople, Gaussian, Inc., Wallingford CT, (2004).

[9] G. Schaftenaar, J.H. Noordik, J. Comput. Aided Mol. Des. 14 (2000) 123.

[10] H.M. McConnell, J. Chem. Phys. 35 (1961) 508;
R. Hoffmann, Acc. Chem. Res. 4 (1971) 1;
M.D. Newton, Int. J. Quantum Chem. 77 (2000) 255;
K.D. Jordan, M.N. Paddon-Row, Chem. Rev. 92 (1992) 395;
B.P. Paulson, L.A. Curtiss, B. Bal, G.L. Closs, J.R. Miller, J. Am. Chem. Soc. 118 (1996) 378.

[11] We defined the centroid of the $-NH_3$ group-localized orbital to be on the contour line within which 60% of that Rydberg orbital's integrated electron density resides and, on this contour, at the furthest distance from the S—S midpoint.

[12] Of course, this speed is a classical quantity whereas the true S—S bond motion is governed by quantum mechanics. Moreover, this is only the average speed; the speed is higher near the mid-point of the vibration and lower near the turning points.